6-3

3D MOSFET Simulation Considering Long-Range Coulomb Potential Effects for Analyzing Statistical Dopant-Induced Fluctuations Associated with Atomistic Process Simulator

Tatsuya Ezaki, Takeo Ikezawa, Akio Notsu, Katsuhiko Tanaka, and Masami Hane

Silicon Systems Research Laboratories, NEC Corporation,
1120 Shimokuzawa, Sagamihara, 229-1198, Japan
E-mail: t-ezaki@ap.jp.nec.com

Abstract – **We have developed a realistic 3-D process/device simulation method for investigating the fluctuation in device characteristics induced by the statistical nature of the number and position of discrete dopant atoms. We used it to investigate the variations in characteristics of a sub-100nm CMOS device induced by realistic dopant fluctuations considering practical device fabrication processes. In particular, sensitivity analysis of the threshold voltage fluctuation was performed in terms of the independent dopant contribution, such as that of the dopant in the source/drain region or channel region.**

I. Introduction

As MOSFET scaling has approached the sub-100nm range, the number of dopants has reached the order of hundreds in the depletion region, and below 100 in the inversion layer. As a result, "intrinsic" fluctuation in device characteristics due to discrete dopant atoms has become a serious problem in ultra-small MOSFETs [1]. The realistic modeling of dopant-fluctuation effects in deep sub-100nm MOSFETs requires three-dimensional (3-D) device simulation coupled with predictive atomistic process simulation. Previous papers related to device-fluctuation simulation [1], however, had little discussion of realistic dopant fluctuation. In this work, we have investigated intrinsic device fluctuation using a 3-D drift-diffusion (DD) device simulator [2] enhanced to treat discrete positions of ionized impurity atoms obtained from an atomistic Monte Carlo (MC) process simulator [3] (Fig. 1).

II. Simulation Method

The discrete dopant distributions in MOSFETs are calculated using atomistic process (ion implantation/activation) simulation (Fig. 2) [3]. The predictive capability of this simulation is based on its incorporation of boron activation kinetics obtained through *ab-initio* calculation. The statistical nature of the discrete dopant distributions can be automatically included by using the MC procedure for both ion implantation and diffusion/activation. The important point when studying the fluctuations in device characteristics lies in how we introduce the microscopic nonuniformity of a discrete dopant distribution into the device simulator. Simply assigning a point charge to each ionized impurity atom site often causes a singularity problem in the potential profile, which leads to a nonphysical carrier localization around the impurity atoms (Fig. 3). This results in nonphysical charge compensation even in depletion regions. To avoid this, we divided the atomistic Coulomb potential into long- and short-range parts, and then used the long-range part to construct an atomistic potential distribution.

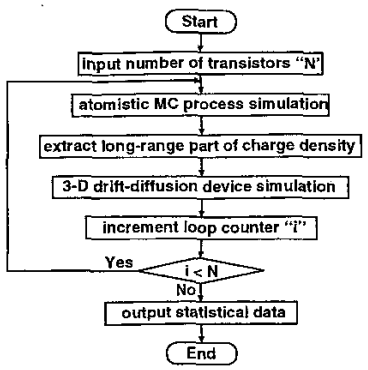

Figure 1: Flowchart of 3-D device simulation coupled with atomistic MC process simulation. Discrete dopant positions are determined by atomistic process simulation. Potential profile in device simulator is calculated by incorporating discrete dopant atom placement. Intrinsic device fluctuations are obtained by iteration.

The long-range part of the charge density, $\rho(r)$, of a single point charge located at the origin ($r = 0$) can be derived from the Fourier expansion of the delta function by removing the high-frequency components [4]. It is expressed as

$$\rho(r) = \frac{ek_c^3}{2\pi^2}\frac{\sin(k_c r) - (k_c r)\cos(k_c r)}{(k_c r)^3}, \qquad (1)$$

where k_c is the reciprocal screening length. The corresponding potential is given by

$$\phi(r) = -\frac{ek_c}{2\pi^2\varepsilon}\frac{\mathrm{Si}(k_c r) - k_c r\sin(k_c r)}{k_c r}. \qquad (2)$$

The cosine term in Eq. (1) should be omitted because otherwise it could cause a convergence problem in actual device simulation due to the relatively large potential oscillation, as shown in Fig. 4. The convergence problem was avoided by removing the cosine term. The long-range parts of the charge density and potential used in our device simulator are then expressed as

$$\rho(r) = \frac{ek_c^3}{2\pi^2}\frac{\sin(k_c r)}{(k_c r)^3} \qquad (3)$$

$$\phi(r) = -\frac{ek_c}{2\pi^2\varepsilon}\frac{\mathrm{Si}(k_c r)}{k_c r}. \quad (4)$$

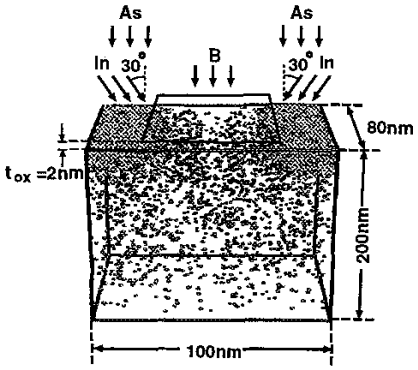

Figure 2: Simulation domain, dopant type, and discrete dopant positions calculated using atomistic MC process simulation. Spike annealing at 1050°C was used as the thermal diffusion process. The gate length was 70nm, and the gate-oxide thickness was 2nm.

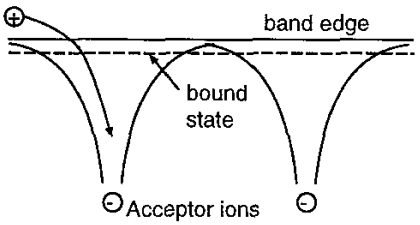

Figure 3: Schematic diagram of electric potential profile formed by negatively charged acceptors. Holes are deeply trapped by the bare Coulomb potential, leading to non-physical charge compensation even in depletion regions.

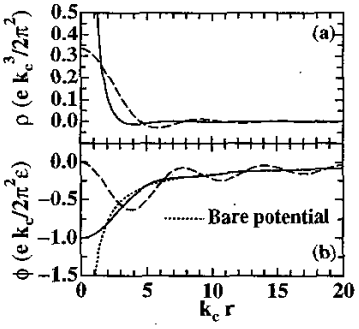

Figure 4: Long-range parts of (a) charge density and (b) corresponding potential profile. Solid lines show charge density and potential profile used in device simulation (Eqs. (3) and (4)). Broken lines show the model proposed by Sano *et al.* [4]. Broken line in (b) shows relatively large oscillation arising from cosine term in density profile (Eq. (1)). Short-range part causes divergence in potential profile (dotted line in (b)).

Since the device fluctuation depends on the screening length (Fig. 5), predictive simulation of ultra-small MOSFET operation requires a physically appropriate value of the screening length. This value was derived from the experimental relationship between electron mobility and impurity concentration by performing a full-band (FB) ensemble Monte Carlo (EMC) simulation for bulk silicon coupled with molecular dynamics (MD) (Figs. 6 and 7). In the FB EMC/MD simulation, electron-phonon scattering and impact ionization were calculated in terms of the FBMC method, and the MD approach was used to simulate the Coulombic interactions between electrons. Electron mobility was determined by averaging electron group velocity from over a few-10ps up to 100ps. Using our physically meaningful screening length, we can reasonably introduce the long-range Coulombic interaction between carriers and impurity atoms into DD device simulation.

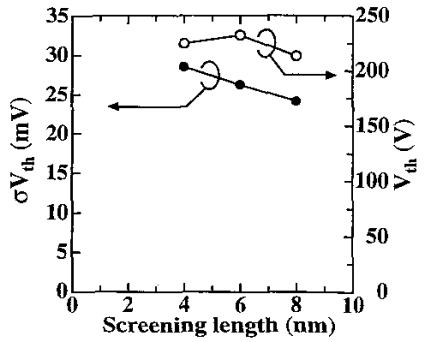

Figure 5: Simulated σV_{th} and $\langle V_{\mathrm{th}} \rangle$ as a function of screening length: σV_{th} decreased with increase in screening length, whereas $\langle V_{\mathrm{th}} \rangle$ showed no clear dependency.

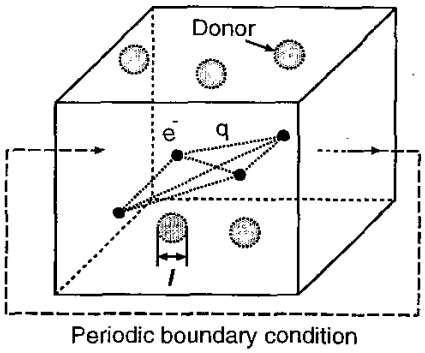

Figure 6: Schematic illustration of FB EMC/MD simulation; l is screening length of impurity charges, as in Eqs. (1) and (2). In the MD calculation, Coulomb force between all electron-pairs was updated in small time steps, typically 0.001fs, and a periodic boundary condition was used for all boundaries.

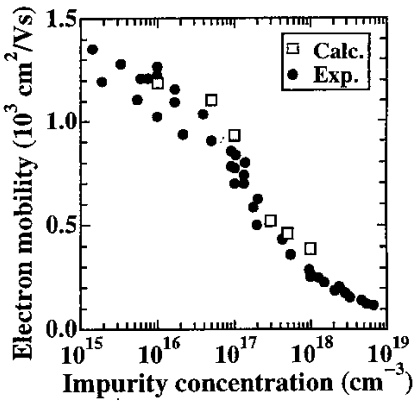

Figure 7: Electron mobility in bulk silicon as function of impurity concentration. Solid circles and open rectangles show experimental [5] and simulation results, respectively. Electron mobility was calculated using FB EMC/MD simulation taking many body Coulombic interactions into account. Screening length was determined as 4nm.

III. Results and Discussion

Performing over 100 MC process simulations of a realistic process recipe for a typical sub-100 nm CMOS (Fig. 2), we evaluated the fluctuations in threshold voltage ($V_{\rm th}$) and $I_{\rm d}$-$V_{\rm g}$ characteristics for both p- and n-MOSFETs within a single IC chip containing microscopically different transistors (Figs. 8 – 10). In particular, we confirmed that our simulation method can reproduce the threshold voltage fluctuation of practical MOSFET devices. Comparison between the results of our physics-based dopant distribution case and a three-dimensional Poisson distribution case (using the same device geometry and dopant profile) (Fig. 11) showed that the average value of $V_{\rm th}$ ($\langle V_{\rm th}\rangle$) and the standard deviation of $V_{\rm th}$ ($\sigma V_{\rm th}$) were identical in both cases (Fig. 12). This means the statistical nature of a discrete dopant can be captured with a 3D Poisson distribution.

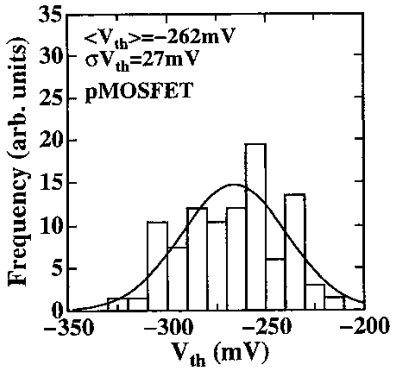

Figure 8: $V_{\rm th}$ frequency distribution and corresponding normal distribution for pMOSFET. Standard deviation of $V_{\rm th}$ was found to be 27mV.

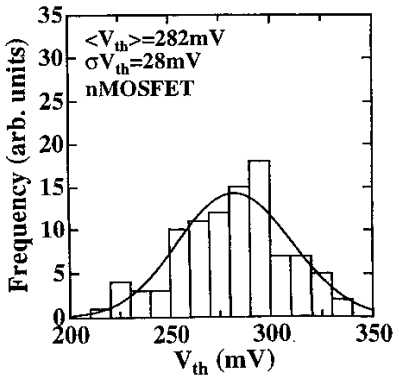

Figure 9: $V_{\rm th}$ frequency distribution and corresponding normal distribution for nMOSFET. Standard deviation of $V_{\rm th}$ was found to be 28mV.

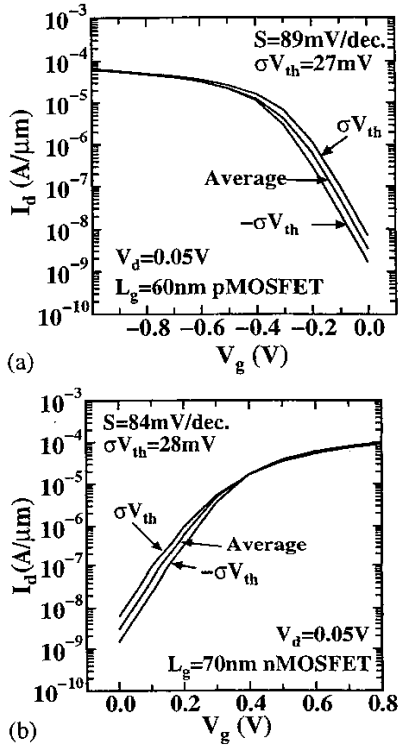

Figure 10: Fluctuation in $I_{\rm d}$-$V_{\rm g}$ characteristics for (a) pMOSFET and (b) nMOSFET with microscopically different impurity distributions calculated using atomistic process and 3-D device simulation. Graphs show $I_{\rm d}$-$V_{\rm g}$ characteristics at the $\langle V_{\rm th}\rangle$ and $\langle V_{\rm th}\rangle \pm \sigma V_{\rm th}$ points. Variations in subthreshold swing were not identified for either p- or n-MOSFETs.

Our atomistic approach for both process and device simulation enables us to perform sensitivity analysis for $\sigma V_{\rm th}$ in terms of independent dopant contributions such as that of the dopant in the source/drain (S/D) region or channel region. The $\sigma V_{\rm th}$ induced by the specific dopant fluc-

tuation was calculated assuming zero fluctuation for certain dopant positions (Fig. 13). The $\sigma V_{\rm th}$ excluding the fluctuation arising from the S/D arsenic profile only was nearly equal to that arising from all of the dopant fluctuations. Consequently, the fluctuation in $V_{\rm th}$ is mostly affected by fluctuations in the channel boron and pocket indium distributions.

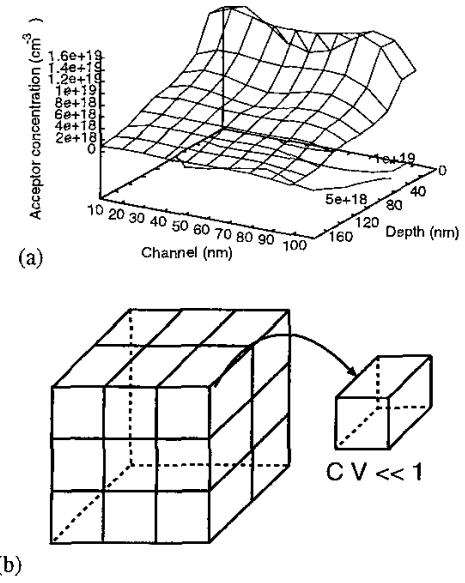

Figure 11: Schematic illustration of random dopant arrangements generated from dopant positions calculated using atomistic process simulation. (a) Continuous impurity distribution generated from discrete dopant positions (Fig. 2) broadened by Gamma function with 4nm half width. (b) Three-dimensional Poisson distribution. Simulation domain was divided into small cells of volume V satisfying $CV \ll 1$, where C is the continuous impurity concentration shown in (a). If the random number is less than CV, an impurity atom is randomly placed in the cell.

IV. Conclusion

We have analyzed fluctuations in device characteristics by using a new 3-D device simulation method associated with predictive atomistic Monte Carlo process simulation. The long-range Coulombic interaction between carriers and ionized impurity atoms was taken into account by using the long-range part of the charge density with a physically appropriate screening length obtained by performing a full-band ensemble Monte Carlo simulation coupled with molecular dynamics. This device simulation method, coupled with the atomistic process simulation, can be used to analyze the individual dopant fluctuation effects on device characteristics and, in particular, can be used to obtain the information needed to optimize device structures and process conditions.

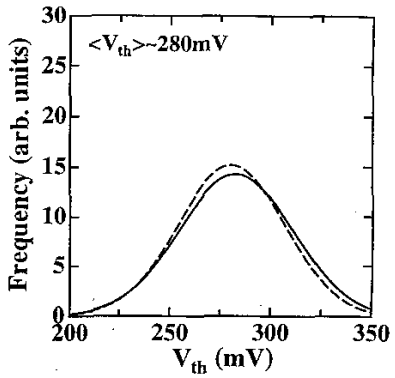

Figure 12: Normal distribution of threshold voltage for sample of 100 microscopically different transistors with artificial random dopant distribution. Solid line shows results obtained from using realistic 3D process/device simulation. Broken line shows results from using 3D Poisson distribution shown in Fig. 11 (b).

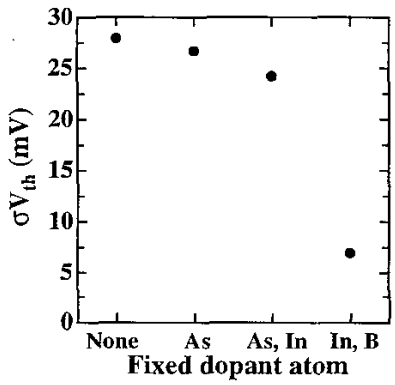

Figure 13: Standard deviation of $V_{\rm th}$ calculated assuming no fluctuations in specified dopant distribution. "None" shows standard deviation when including all dopant fluctuations.

References

[1] A. Asenov, IEEE Trans. Electron Devices **ED-45**, 2505 (1998); D. Vasileska *et al.*, Extended Abstracts IWCE-6, 259 (1998); D. J. Frank *et al.*, VLSI Tech. Dig. 169 (1999).

[2] K. Tanaka *et al.*, NASECODE-6, 317 (1989); K. Tanaka *et al.*, IEICE Trans. Electronics, **E83-C**, 1343 (2000).

[3] M. Hane *et al.*, IEDM Tech. Dig., 843 (2001).

[4] N. Sano *et al.*, IEDM Tech. Dig. 275 (2000).

[5] N. D. Arora *et al.*, IEEE Trans. Electron Devices, **ED-29**, 292 (1982); W. R. Thurber *et al.*, J. Electrochem. Soc., **127**, 1807 (1980).